

Adapting Pre-Trained Vision Models for Novel Instance Detection and Segmentation

Yangxiao Lu, Jishnu Jaykumar P, Yunhui Guo, Nicholas Ruoizzi, and Yu Xiang

Department of Computer Science
University of Texas at Dallas
Richardson, TX 75080, USA

{yangxiao.lu, jishnu.p, yunhui.guo, nicholas.ruozzi, yu.xiang}@utdallas.edu

Abstract

Novel Instance Detection and Segmentation (NIDS) aims at detecting and segmenting novel object instances given a few examples of each instance. We propose a unified framework (NIDS-Net) comprising object proposal generation, embedding creation for both instance templates and proposal regions, and embedding matching for instance label assignment. Leveraging recent advancements in large vision methods, we utilize the Grounding DINO and Segment Anything Model (SAM) to obtain object proposals with accurate bounding boxes and masks. Central to our approach is the generation of high-quality instance embeddings. We utilize foreground feature averages of patch embeddings from the DINOv2 ViT backbone, followed by refinement through a weight adapter mechanism that we introduce. We show experimentally that our weight adapter can adjust the embeddings locally within their feature space and effectively limit overfitting. This methodology enables a straightforward matching strategy, resulting in significant performance gains. Our framework surpasses current state-of-the-art methods, demonstrating notable improvements of 22.3, 46.2, 10.3, and 24.0 in average precision (AP) across four detection datasets. In instance segmentation tasks on seven core datasets of the BOP challenge, our method outperforms the top RGB methods by 3.6 AP and remains competitive with the best RGB-D method¹.

1 Introduction

Novel Instance Detection and Segmentation (NIDS) is a crucial task in computer vision aimed at identifying and locating unseen instances in images or videos, given a few examples of each instance. Of particular interest in this work, are applications of NIDS in robotics, e.g., a robot might need to fetch a specific, novel object instance from a cluttered desk given only a small number of multi-view template images of the novel object. Ideally, detectors for this task should provide precise bounding boxes and masks of the target instances in a cluttered query image, but standard detection systems, trained on specific classes, often struggle to recognize new objects.

The current paradigm for NIDS typically encompasses the following steps: (1) generating proposals from a query image, (2) obtaining embeddings of the proposals and the target instance templates, and (3) matching the embeddings of proposals with those of the templates for identification. Recent work [45, 79, 64, 49] has utilized various open-world detectors to obtain object proposals. However, the use of models such as the Segment Anything Model (SAM) [43] or FastSAM [101] often results in the generation of region-based proposals rather than actual *object* proposals. This misidentification

¹Code is available at: <https://github.com/YoungSean/NIDS-Net>

of regions as objects can lead to object identification issues. For example, a single object may be divided into multiple proposals or some background regions may be mistaken for foreground objects. These false alarms not only slow down the whole detection progress but also spoil the final results. To represent proposals and templates, Shen et al. [79], Nguyen et al. [64], and Lin et al. [49] adopt the *cls* token of DINOv2 [66, 20] while Li et al. [45] employ a 3D voxel representation. Ideally, for each specific unseen instance, the template embeddings from different views should be similar to each other but markedly different from the embeddings of other instances. Despite these efforts, the challenge persists that the embeddings of different instances remain excessively similar. The development of robust feature embeddings could provide a solution to this issue.

To address the limitations of current methods, we propose a framework for NIDS. Initially, we utilize Grounding DINO [52] with the text prompt “objects” on a cluttered query image to obtain bounding boxes for foreground objects. This method capitalizes on the inherent objectness of Grounding DINO using specialized prompts rather than standard labels. Subsequently, we employ SAM to create masks within these bounding boxes, generating precise object proposals comprising both bounding boxes and masks. For instance embeddings, we first extract average foreground features from the patch embeddings of the DINOv2 ViT backbone. We then apply adapters to enhance instance embeddings by clustering similar instances and distancing different ones. The adapters are trained with instance template embeddings via InfoNCE loss [65, 15]. To refine these embeddings, the CLIP-Adapter [28] introduces a residual vector added to the original embedding, which risks overfitting with a few training examples. This addition can spoil and destabilize the embeddings of background objects, disrupting the entire feature space. To mitigate this issue, we introduce a weight adapter that modifies the original embeddings by applying learned weights. Finally, we employ a straightforward matching approach [60], such as stable matching or using *argmax*, to assign instance labels to these proposals.

Our approach has been validated on four detection datasets and seven segmentation datasets. The framework significantly surpasses existing state-of-the-art methods: it demonstrates substantial increases in average precision (AP), with gains of 22.3, 46.2, 10.3, and 24.0 across these detection datasets. Moreover, in instance segmentation tasks on the seven core datasets of the BOP challenge [82], our method outperforms the best RGB and RGB-D methods.

Our contributions are summarized as follows.

- We propose NIDS-Net, a unified framework for novel instance detection and segmentation that surpasses existing methods across four detection datasets and seven segmentation datasets of BOP challenge.
- We leverage the objectness of open-world detector Grounding DINO and region recognition of Segmentation Anything Model (SAM) to obtain object proposals.
- We introduce the Weight Adapter, a tool designed to refine embeddings within their feature space while discouraging overfitting. This approach yields increasingly significant improvements as the adapting of the feature space becomes more robust and stable.

2 Related Work

Pretrained models. Large-scale pretraining has demonstrated utility across various downstream tasks. Works such as [32, 90, 55, 24, 54, 10, 66] emphasize large-scale image representation learning, while [72, 46] focus on vision-language pretraining. Additionally, [3, 4, 95] address depth prediction, and [70, 71, 6, 84] tackle large-scale language modeling. Object detection is addressed by [30, 77, 75, 40, 41, 31, 52], while image segmentation is the focus of [33, 86, 42]. Works such as [93, 48, 14, 74] explore text-to-3D generation, and [80, 1] address text-to-video synthesis. Finally, 6DoF pose estimation and tracking are tackled by [87, 21, 47, 85]. These foundational models offer diverse capabilities, with the challenge lying in effectively leveraging their wealth of knowledge for specific use cases, such as novel instance detection. DINOv2 [66, 20] offers robust features to represent unseen instances.

Open-world object detection (OWOD). OWOD tackles real-world scenarios where object detection algorithms are tasked not only with identifying known and labeled objects but also with effectively handling novel and unknown objects absent during inference. This sets OWOD apart from traditional object detection, which confines itself to detecting only predetermined object classes. A key challenge in OWOD lies in detecting and classifying unknown objects that were not part of the training data. Recent approaches such as OWL-ViT [63], DITO [40], RO-ViT [41], YOLO-World [18], Sambor [31],

and Grounding DINO [52] offer diverse solutions to address OWO challenges. OWL-ViT leverages a standard Vision Transformer [24] architecture with minimal modifications, incorporating contrastive image-text pre-training and end-to-end detection fine-tuning. DITO introduces an open-vocabulary detection approach based on detection-oriented image-text pretraining, replacing the classification architecture with a detector architecture during pretraining to better serve region-level recognition needs. RO-ViT proposes cropping and resizing regions of positional embeddings (PE) at pretraining, aligning better with region-level detection fine-tuning. YOLO-World enhances YOLO [75] with open vocabulary detection capabilities through vision-language modeling and large-scale pretraining. Grounding DINO [52] utilizes features from DINO [10] to ground text queries, while Sambor extends SAM [42] to detect arbitrary objects based on human inputs such as category names or reference expressions. We employ Grounding DINO due to its strong performance.

Few-shot object detection (FSOD). FSOD involves detecting occurrences of a novel class, unseen during training, given only a few template examples. De-ViT [100] introduces a region-propagation mechanism for localization, transforming propagated region masks into bounding boxes using a learnable spatial integral layer. FS-DETR [7], the first few-shot detection transformer, extends DETR [9] to process arbitrary numbers of novel objects concurrently while supporting various examples from each class. Other approaches such as [27] prioritize salient representations through angle distance and magnitude dispersion across few-shot samples, [92] leverages variational autoencoders for data augmentation, and [59] learns geometry-aware features with an offline simplex equiangular tight frame classifier. Additionally, [56] generates specific and representative prototypes for each query image, considering both support and query image features.

Instance detection. Instance detection involves identifying an unseen instance in a test image using corresponding templates. Some methods, e.g., [62, 2, 53], rely on pure 2D representations and matching techniques. Specifically, DTOD [62] employs global object attention and a local pose-specific branch for template-guided heatmap prediction. However, these methods may struggle with variations in 2D appearance caused by occlusion or pose changes. In contrast, VoxDet [45] utilizes explicit 3D knowledge from multi-view templates, providing geometry-invariant representations. We generate 2D robust instance embeddings from templates with DINOv2 [66, 20].

Unseen object instance segmentation (UOIS). UOIS is a task designed to segment unseen objects in cluttered scenes. UOIS generates object masks without providing labels. UOIS-Net [89] utilizes a two-stage framework, initially generating rough masks using depth information, and then refining them into precise instance masks with RGB data. Both UCN [88] and MSMFormer [57, 58] segment objects by clustering pixel embeddings. Although these methods can generate object proposals, they primarily focus on tabletop settings. In contrast, our approach is designed to handle RGB query images in various environments.

Adapter. The application of adapters atop large pre-trained models has emerged as a prominent strategy, yielding significant improvements across various tasks. Previous works have leveraged adapters to enhance few-shot image classification tasks [28, 97, 68, 99, 81]. Other works have demonstrated effectiveness in language model fine-tuning [36, 37, 98, 29]. Additional works exhibit the promise of adapters in vision tasks including detection and segmentation [17, 16, 69, 91, 23]. For novel instance detection and segmentation, we propose the Weight Adapter to enhance performance. The adapter assigns weights to the embeddings from frozen backbones.

3 Method

Novel instance detection and segmentation (NIDS), also referred to as open-world detection and segmentation, is a task to locate and label unseen instances within a query image. We will assume that each of the N target instances is represented by K template images $I_T \in \mathbb{R}^{K \times 3 \times W \times H}$ and their corresponding segmentation masks. During inference, the output of each query image $I_Q \in \mathbb{R}^{3 \times W \times H}$ provides these instances' bounding boxes for detection and instance masks for segmentation.

3.1 Instance Embedding Generation Stage

In our approach, an instance embedding summarizes the pixels of an instance. The objective of this stage is to generate initial instance embeddings. Each of the N instances has K multi-view template images and their ground truth segmentation masks from which we derive template embeddings $E_T \in \mathbb{R}^{N \times K \times C}$, where C is the dimension of the embeddings. Given an image and its corresponding

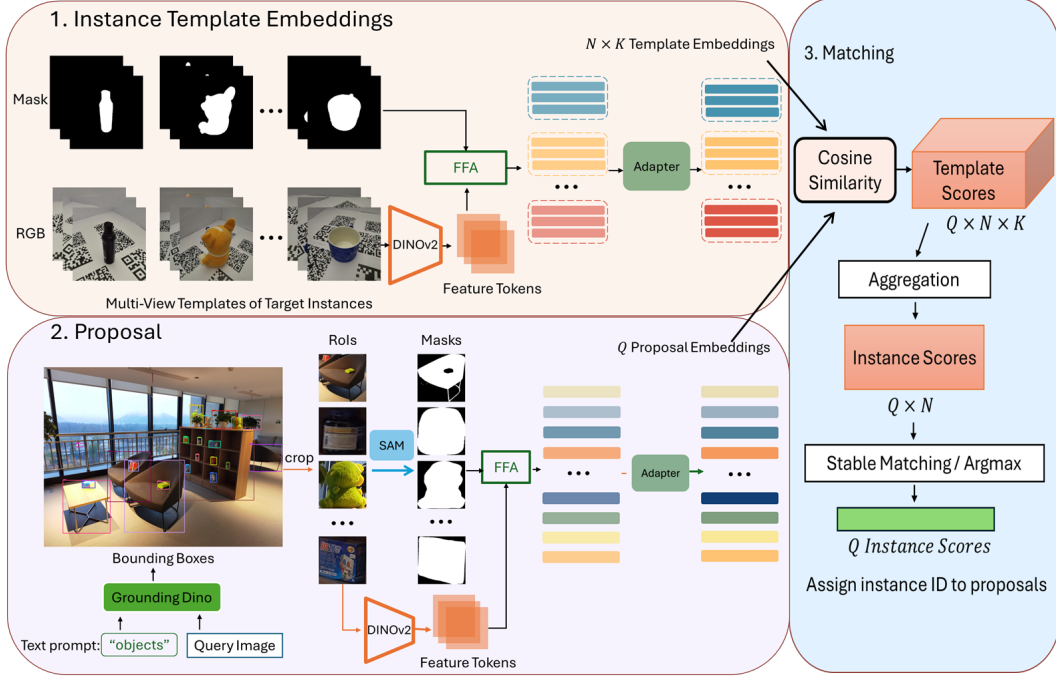


Figure 1: In our framework NIDS-Net, only adapters are learnable, while other models are frozen. Instance IDs are the instance labels.

mask, we initially extract patch embeddings using the ViT backbone of DINOv2, and subsequently obtain foreground features as specified by the mask. We then perform average pooling on these features. This process, termed Foreground Feature Averaging (FFA), is proposed by [44] to assess object similarity. We employ FFA to generate all initial instance embeddings.

3.2 Object Proposal Stage

The purpose of this stage is to acquire object proposals from a query image. Previous studies [79, 64, 49] have utilized SAM [43] or FastSAM [101] to generate regions as object proposals. Such proposals contain a high number of false alarms. For example, SAM might misclassify background regions or parts of objects as complete objects. To address this challenge, an off-the-shelf zero-shot detector, Grounding Dino [52], is employed with the text prompt “objects” to obtain initial bounding boxes of foreground objects. Then, SAM is applied to create masks based on these bounding boxes. The integration of these two models, termed Grounded-SAM (GS) [78], significantly reduces the number of erroneous object proposals and expedites the subsequent stages. Moreover, this approach eliminates the need for training of the detector. We then extract the proposal regions along with their corresponding masks from the query images. Using the FFA pipeline with proposals, we calculate proposal embeddings $E_P \in \mathbb{R}^{Q \times C}$, which correspond to Q regions of interest. Fig. 1 illustrates the process of obtaining proposal embeddings.

3.3 Embedding Refinement via an Adapter

Most instance embeddings are well separated. However, some embeddings from distinct instances may cluster together. For example, background object embeddings might be similar to targets. Some target instances may resemble each other. To address this issue, we employ learnable adapters to refine the embeddings. We train these adapters using InfoNCE loss [65, 15], aiming to bring the embeddings of the same instance closer together while separating the embeddings of different instances.

CLIP-Adapter (CA). CLIP-Adapter [28] comprises two trainable linear bottleneck layers appended to the language and image branches of CLIP. During few-shot fine-tuning, the original CLIP backbone remains frozen. Nonetheless, adding extra layers for fine-tuning may result in overfitting to the few examples available. To mitigate this issue, CLIP-Adapter integrates residual connections that dynamically merge the newly adapted knowledge with the foundational knowledge from the original CLIP backbone.

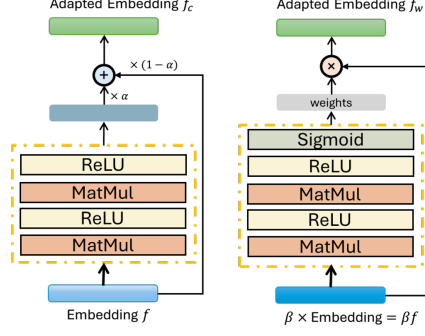


Figure 2: Comparison of two adapters. (left) CLIP-Adapter. (right) Our weight adapter.

Given an instance embedding f and a *MLP* (Multi-Layer Perceptron), the CLIP-Adapter modifies the embedding according to the formula $f_c = \alpha \times MLP(f) + (1 - \alpha) \times f$. In this equation, f_c represents the adapted embedding, which is a linear combination of the transformed embedding $MLP(f)$ and the original embedding f . The residual ratio α is set as 0.6.

Our Weight Adapter (WA). The CLIP-Adapter refines instance embeddings by adding a new feature vector. However, this new vector might not align with the feature space of original instance embeddings, which can lead to overfitting. Since only several hundred template embeddings of target instances are trained and refined in some datasets, the embeddings of background objects can be spoiled as the process disrupts the distances between target and background instance embeddings. Assuming the feature space of original embeddings is robust and effective, it is crucial to fine-tune the instance embeddings within this space by constraining the scope of the adapted embeddings. This refinement can be accomplished by simply applying weights to the original instance embeddings.

Hence, we introduce our Weight Adapter, a compact *MLP* network depicted in Fig. 2. The operation of this adapter is described through the following equations:

$$w = \text{sigmoid}(MLP(\beta f)), \quad (1)$$

$$f_w = w \odot (\beta f). \quad (2)$$

Here, β is a positive scalar. We set β as 10. w is the weights computed by passing the scaled embedding βf through the *MLP* and then applying a *sigmoid* function. The output f_w is the element-wise product of w and the scaled embedding βf , resulting in the weighted embedding.

We include a *ReLU* layer before the *sigmoid* function, ensuring that the *sigmoid*'s output is constrained to the range $[0.5, 1)$. Subsequently, each refined embedding is close to its original counterpart. Additionally, β allows for broader adjustments within the feature space. Given that cosine similarity is utilized to compare embeddings in the subsequent phase, our adapter alters the interrelationships among the values within each embedding. Further details of adapters are presented in Fig. 2. Qualitative results can be found in the appendix.

3.4 Matching Stage

This stage provides each proposal i with an instance ID o_i as its label and a confidence score s_i .

Initially, Q proposal embeddings E_P are matched with $N \times K$ template embeddings E_T using cosine similarity. It yields a matrix of template scores with dimensions $Q \times N \times K$, as illustrated in Fig. 1. For each instance, we aggregate all K template scores to derive a matrix of instance scores with dimensions $Q \times N$. We employ *Max* as the aggregation function for optimal results.

Bonus instance score for segmentation. To improve segmentation performance, we incorporate an additional appearance matching score, s_{appe} , as proposed by SAM-6D [49], into the instance scores. s_{appe} is used to identify objects that are semantically similar yet differ in appearance. For each proposal, we can identify its most similar template T_{best} according to template scores. s_{appe} is derived from the patch embeddings of a proposal image I and T_{best} . It quantifies the similarity between the query image and the template in terms of their local features as follows:

$$s_{\text{appe}} = \frac{1}{N_{\text{patch}}^I} \sum_{j=1}^{N_{\text{patch}}^I} \max_{i=1, \dots, N_{\text{patch}}^{T_{\text{best}}}} \left(\text{CosineSimilarity}(f_{I,j}^{\text{patch}}, f_{T_{\text{best}},i}^{\text{patch}}) \right)$$

Assuming that objects are unique within a query image [79], we employ the stable matching algorithm [60] on instance scores to assign a unique instance ID to each proposal. If the assumption of uniqueness is not met, we use the *Argmax* function on the instance score matrix, which permits multiple proposals to share the same instance ID.

After matching, we acquire labeled proposals. Each is defined by $\{b_i, M_i, o_i, s_i\}$. Here, b_i is the bounding box of an instance. M_i is the modal mask, which covers the visible object surface [82]. o_i is the instance ID. s_i is the confidence score. A confidence score threshold δ can be used to remove incorrect proposals.

4 Experiments

We employ the Grounding DINO model with a Swin-T backbone [52] and a text prompt “objects”, and the default ViT-H SAM [43] to generate object proposals. According to the proposals, we obtain the regions of interest (RoIs) and resize them to 448×448 or 224×224 resolutions. For object detection, instance embeddings are produced using the DINOv2’s ViT-L model with registers [20], employing stable matching due to the uniqueness of instances in these datasets. For image segmentation, following SAM-6D [49], we utilize the ViT-L model of DINOv2 [66]. In scenarios with identical instances, such as the cluttered scenes in BOP datasets, we apply the *argmax* function for matching.

The experiments are conducted on an RTX A5000 GPU. For each dataset, we train both adapters on template embeddings using InfoNCE loss [65, 15] with temperature 0.05. With two linear layers, Both adapters initially decrease the embedding dimension from C to $C/4$, subsequently restoring it to C . The Weight Adapter is trained with Adam optimizer at a learning rate of $1e-3$ and a batch size of 1024, while the CLIP-Adapter is trained at a learning rate of $1e-4$. Dropout is incorporated in the CLIP-Adapter to reduce overfitting. For additional details, please see the Appendix.

4.1 Detection Datasets

We utilize recently developed instance detection datasets and their associated baselines [79, 45]. The High-resolution and RoboTools datasets employ real template images, while the LM-O and YCB-V datasets utilize synthetic images.

High-resolution dataset Shen et al. [79] design a high-resolution dataset for instance detection. This dataset comprises 100 distinct object instances, each represented by 24 photos taken from multiple viewpoints, with each photo having a resolution of 3072×3072 pixels. These instances are integrated into 14 different indoor scenes for testing, captured in even higher resolution (6144×8192 pixels). The testing images are further classified as easy or hard based on the level of scene clutter and how much the instances are occluded. Easy tags are assigned when objects are sparsely placed, while hard tags are used for more cluttered setups.

Baselines According to Shen et al. [79], two types of baselines are set for the high-resolution dataset: Cut-Paste-Learn and a non-learned method. Cut-Paste-Learn generates synthetic training images with 2D-box annotations, putting foreground instances in various sizes and aspect ratios onto different backgrounds. This enables training detectors by viewing each instance as a class. They train five detectors: FasterRCNN [76], RetinaNet [51], CenterNet [102], FCOS [83], and the transformer-based DINO [96]. For the non-learned method, SAM is initially used to generate proposals, followed by employing DINO [11] and DINOv2 [66] to generate features for both proposal and template images, ultimately performing proposal matching and selection.

Synthetic-Real test sets Li et al. [45] employ two benchmarks for evaluation. LineMod-Occlusion (LM-O) [5] includes 8 texture-less objects and 1,514 bounding boxes, primarily challenging due to significant occlusion. The YCB-Video (YCB-V) [8] features 21 objects and 4,125 bounding boxes, with pose variation as the main challenge. Since these datasets have real testing images without reference videos, Li et al. [45] generate synthetic videos using CAD models. We sample 16 synthetic template images per object from these videos.

RoboTools benchmark Li et al. [45] introduce RoboTools, a challenging real-world benchmark for robotics. It features 20 distinct instances, 9,109 annotations, and 24 complex scenarios. Compared to previous benchmarks [5, 8], RoboTools offers greater difficulty due to its cluttered backgrounds and significant pose variations. Additionally, the benchmark’s reference videos are made from real images and incorporate realistic lighting conditions, including shadows. 25 real template images of each instance are sampled from reference videos.

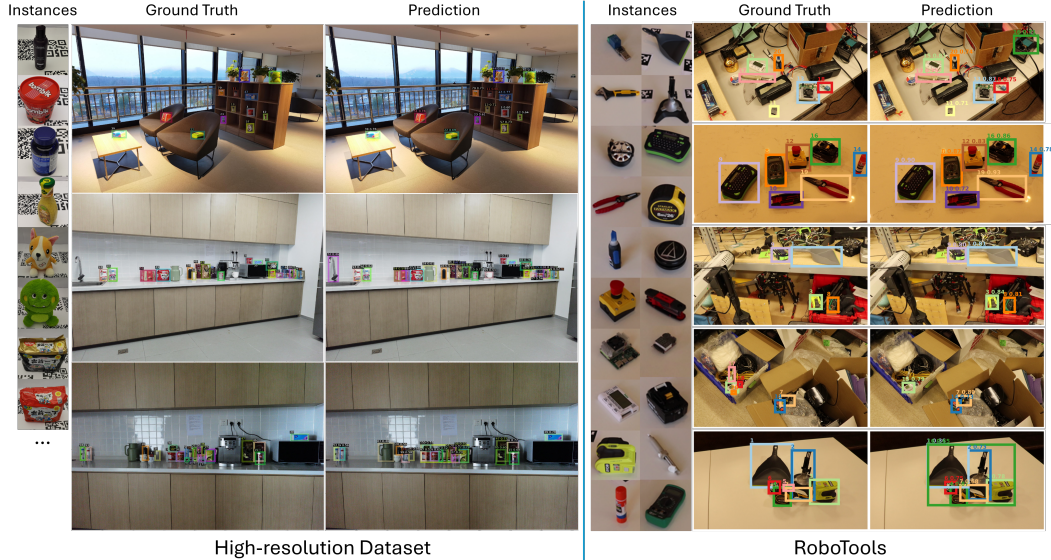


Figure 3: Visual examples of our results using the Weight Adapter on the high-resolution and RoboTools datasets. Our approach detects specific object instances in cluttered scenes according to their real template images.

Baselines For cluttered scenes from the datasets RoboTools, LM-O and YCB-V, Li et al. [45] have developed several 2D baselines: OLN_{DINO} , OLN_{CLIP} , and OLN_{Corr} . Initially, they generate open-world 2D proposals using their detection module [39]. For matching, different methods are employed to select the proposal with the highest score. In OLN_{DINO} and OLN_{CLIP} , they use robust features from pre-trained backbones [11, 73] and cosine similarity for matching. For OLN_{Corr} , a matching head is designed based on correlation [53]. They also employ the class-level one-shot detectors OS2D [67] and BHRL [94]. To address the limitations of traditional 2D methods with pose variations and occlusions, Li et al. [45] introduced VoxDet which is based on a 3D voxel representation. To train these methods, Li et al. [45] developed the open-world instance detection (OWID-10k) dataset as a synthetic instance detection training set. It features 9,901 objects from ShapeNet [12] and ABO [19], each rendered into a 40-frame, 360-degree video using Blenderproc [22].

Evaluation metrics For detection, we evaluate our method with Average Precision (AP). AP is computed by averaging precision scores at various Intersection over Union (IoU) thresholds, specifically from 0.5 to 0.95, in increments of 0.05. This metric is the primary evaluation standard in the COCO Object Detection dataset [50]. Additionally, AP50 and AP75 are variations of this metric, where precision is averaged across all instances at IoU thresholds of 0.5 and 0.75, respectively.

4.2 Segmentation Datasets

BOP challenge We test our method using seven datasets from the BOP challenge [82]: LineMod Occlusion (LM-O) [5], T-LESS [34], TUD-L [35], IC-BIN [25], ITODD [26], HomebrewedDB (HB) [38], and YCB-Video [8]. The objects from these datasets vary widely. We use 42 template rendering images from CNOS [64], which are generated via BlenderProc [22].

Baselines We compare our method with ZeroPose [13], CNOS [64], and SAM-6D [49]. These methods utilize proposals from SAM [43] or FastSAM [101] and use the cls token from DINOv2 as the instance embedding for matching. In addition to adjusting the SAM hyperparameters to generate more proposals, SAM-6D enhances its performance by incorporating an appearance score, s_{appe} . Moreover, SAM-6D employs a Geometric Matching Score, s_{geo} , which considers the shapes and sizes of instances during matching by utilizing depth information.

Evaluation metrics For instance segmentation task, we evaluate our method using the Average Precision (AP) metrics. The AP is computed by averaging the precision scores at various IoU thresholds, from 0.50 to 0.95, increasing by 0.05 at each step.

4.3 Benchmarking Results

Table 1: Detection results on the high-resolution dataset. *avg* indicates that we are evaluating all images, including those from the easy and hard scenes. We train these two adapters with 2400 template embeddings.

| Method | AP | | | | | | AP ₅₀ | AP ₇₅ | Time (sec) |
|--------------------------------|-------------|-------------|-------------|-------------|-------------|-------------|------------------|------------------|------------|
| | avg | hard | easy | small | medium | large | | | |
| FasterRCNN [76] | 19.5 | 10.3 | 23.8 | 5.0 | 22.2 | 38.0 | 29.2 | 23.3 | 0.00399 |
| RetinaNet [51] | 22.2 | 14.9 | 26.5 | 5.5 | 25.8 | 42.7 | 31.2 | 25.0 | 0.00412 |
| CenterNet [102] | 21.1 | 11.8 | 25.7 | 5.9 | 24.1 | 40.4 | 32.7 | 23.6 | 0.00376 |
| FCOS [83] | 22.4 | 13.2 | 28.7 | 6.2 | 26.5 | 38.1 | 32.8 | 25.5 | 0.00271 |
| DINO [96] | 28.0 | 17.9 | 32.6 | 11.5 | 30.7 | 45.1 | 32.2 | 32.2 | 1.90625 |
| SAM + DINO _f [11] | 37.0 | 22.4 | 43.9 | 11.9 | 40.9 | 62.7 | 44.1 | 40.4 | 15.10 |
| SAM + DINOv2 _f [66] | 41.6 | 28.0 | 47.6 | 14.6 | 45.8 | 69.1 | 49.1 | 46.0 | 14.70 |
| NIDS-Net (Ours) | 59.3 | 41.7 | 67.4 | 12.7 | 58.1 | 78.8 | 71.1 | 65.1 | 6.92 |
| NIDS-Net + CA (Ours) | 61.3 | 42.5 | 69.6 | 17.0 | 59.3 | 81.6 | 73.2 | 67.0 | 6.99 |
| NIDS-Net + WA (Ours) | 63.9 | 43.4 | 72.7 | 18.1 | 62.5 | 84.0 | 76.6 | 70.6 | 6.78 |

Table 3: Detection performance on the LM-O and YCB-V datasets. OLN* is trained alongside the matching head whereas OLN uses fixed modules. † means the model is trained on OWID and real images. Our running time of YCB-V is based on the scene 48. (·) represents the number of instances.

| Method | Proposal | Train | LM-O (8) | | | YCB-V (21) | | | Average | | | Time (s) |
|------------------------------|----------|-------|-------------|------------------|------------------|-------------|------------------|------------------|-------------|------------------|------------------|----------|
| | | | AP | AP ₅₀ | AP ₇₅ | AP | AP ₅₀ | AP ₇₅ | AP | AP ₅₀ | AP ₇₅ | |
| OS2D [67] | N/A | OWID | 0.2 | 0.7 | <0.1 | 5.2 | 18.3 | 1.9 | 2.7 | 9.5 | 1.0 | 0.189 |
| DTOD [61] | N/A | OWID | 9.8 | 28.9 | 3.7 | 16.3 | 48.8 | 4.2 | 13.1 | 38.9 | 4.0 | 0.357 |
| OLN _{CLIP} [39, 73] | OLN | OWID† | 16.2 | 32.1 | 15.3 | 10.7 | 25.4 | 7.3 | 13.5 | 28.8 | 11.3 | 0.357 |
| Gen6D [53] | N/A | OWID† | 12.0 | 29.8 | 6.6 | 8.1 | 33.0 | 5.5 | 18.4 | 33.5 | 5.9 | 0.769 |
| BHRL [94] | N/A | COCO | 14.1 | 21.0 | 15.7 | 31.8 | 47.0 | 34.8 | 23.0 | 34.0 | 25.3 | N/A |
| OLN _{Corr} [39, 53] | OLN* | OWID | 22.3 | 34.4 | 24.7 | 24.8 | 41.1 | 26.1 | 23.6 | 37.8 | 25.4 | 0.182 |
| OLN _{Dino} [39, 11] | OLN | OWID† | 23.6 | 41.6 | 24.8 | 25.6 | 53.0 | 21.1 | 24.6 | 47.3 | 23.0 | 0.357 |
| VoxDet [45] | OLN* | OWID | 29.2 | 43.1 | 33.3 | 31.5 | 51.3 | 33.4 | 30.4 | 47.2 | 33.4 | 0.154 |
| NIDS-Net (Ours) | GS | N/A | 38.7 | 66.0 | 41.0 | 53.0 | 72.9 | 61.7 | 45.9 | 69.5 | 51.4 | 3.73 |
| NIDS-Net + CA (Ours) | GS | N/A | 39.2 | 67.0 | 41.4 | 53.9 | 74.1 | 62.7 | 46.6 | 70.6 | 52.1 | 3.71 |
| NIDS-Net + WA (Ours) | GS | N/A | 39.5 | 67.4 | 41.8 | 55.5 | 75.5 | 65.0 | 47.5 | 71.5 | 53.4 | 3.73 |

Table 2: Detection performance on the fully real dataset, RoboTools. **Proposal** indicates the object proposal model. *GS* stands for Grounded-SAM. OLN* is trained with the matching head while OLN employs fixed modules.

| Method | Proposal | AP | AP ₅₀ | AP ₇₅ |
|------------------------------|----------|-------------|------------------|------------------|
| OS2D [67] | N/A | 2.9 | 6.5 | 2.0 |
| DTOD [61] | N/A | 3.6 | 9.0 | 2.0 |
| OLN _{Corr} [39, 53] | OLN* | 14.4 | 18.1 | 15.7 |
| VoxDet [45] | OLN* | 18.7 | 23.6 | 20.5 |
| NIDS-Net (Ours) | GS | 63.3 | 77.2 | 68.7 |
| NIDS-Net + CA (Ours) | GS | 64.8 | 79.2 | 70.7 |
| NIDS-Net + WA (Ours) | GS | 64.9 | 79.4 | 70.8 |

Detection The high-resolution dataset results are presented in Table 1. Our models dramatically outperform existing techniques, achieving the highest AP scores across all categories. Our basic method surpasses the top baseline by 17.7 AP. Additionally, as this dataset contains 100 instances with some similarities among them, our Weight Adapter boosts overall performance by 4.6 AP and improves the detection of small objects by 5.4 AP. For the RoboTools dataset, detailed in Table 2, our method outperforms the state-of-the-art VoxDet by 46.2 AP. Since RoboTools contains only 20 instances, our

adapter has limited scope to enhance performance. Our approach achieves over 60 AP on these two fully real datasets.

For the Synthetic-Real datasets, LM-O and YCB-V, we present a comparison of our approach with other methods in Table 3. Our model outperforms VoxDet by 10.3 AP on LM-O and by 24.0 AP on YCB-V. The improved performance on YCB-V, which contains more instances, indicates that our adapter functions more effectively with increased instance variety.

Segmentation CNOS [64] and SAM-6D [49] initially utilize SAM or FastSAM to obtain proposals and derive instance embeddings through the *cls* token of Dinov2. In contrast, we generate proposals using Grounded-SAM and acquire embeddings through the FFA pipeline. The segmentation results for the seven principal datasets of the BOP challenge are detailed in Table 4. Overall, our method surpasses the state-of-the-art SAM-6D and achieves superior results compared to RGBD results.

Qualitative result We present detection results for both simple and complex scenes in Fig. 3. Additional detection and segmentation examples are available in the Appendix.

Runtime The tables of detection results include the runtime of our method. Despite Grounded-SAM reducing the number of proposals, our approach remains slower compared to end-to-end detectors. This is primarily due to the process involved in obtaining proposal embeddings. The inclusion of adapters does not impede the overall framework. Future research could focus on developing a more efficient method for robotic applications. Please see the appendix for segmentation runtime.

Table 4: Novel instance segmentation results on the seven core datasets of the BOP benchmark. We utilize Average Precision (AP) to compare these methods. (·) includes the number of instances.

| Method | BOP Datasets | | | | | | | Mean |
|---|--------------|-------------|-------------|-------------|-------------|-------------|-------------|-------------|
| | LM-O (8) | T-LESS (30) | TUD-L (3) | IC-BIN (2) | ITODD (28) | HB (33) | YCB-V (21) | |
| ZeroPose (SAM) [13] | 34.4 | 32.7 | 41.4 | 25.1 | 22.4 | 47.8 | 51.9 | 36.5 |
| CNOS (SAM) [64] | 39.6 | 39.7 | 39.1 | 28.4 | 28.2 | 48.0 | 59.5 | 40.4 |
| CNOS (FastSAM) [64] | 39.7 | 37.4 | 48.0 | 27.0 | 25.4 | 51.1 | 59.9 | 41.2 |
| SAM-6D (FastSAM) [49] | 39.5 | 37.6 | 48.7 | 25.7 | 25.3 | 51.2 | 60.2 | 41.2 |
| SAM-6D (FastSAM) + s_{apoc} [49] | 40.6 | 39.3 | 50.1 | 27.7 | 29.0 | 52.2 | 60.6 | 42.8 |
| SAM-6D (SAM) [49] | 43.4 | 39.1 | 48.2 | 33.3 | 28.8 | 55.1 | 60.3 | 44.0 |
| SAM-6D (SAM) + s_{apoc} [49] | 44.4 | 40.8 | 49.8 | 34.5 | 30.0 | 55.7 | 59.5 | 45.0 |
| SAM-6D (SAM, <i>RGBD</i>) [49] | 46.0 | 45.1 | 56.9 | 35.7 | 33.2 | 59.3 | 60.5 | 48.1 |
| NIDS-Net (Ours) | 42.9 | 43.0 | 52.0 | 30.5 | 28.8 | 56.6 | 59.7 | 44.8 |
| NIDS-Net + CA (Ours) | 42.8 | 47.5 | 50.0 | 29.7 | 27.6 | 62.7 | 63.5 | 46.3 |
| NIDS-Net + WA(Ours) | 43.2 | 49.2 | 53.5 | 30.5 | 29.4 | 62.4 | 64.3 | 47.5 |
| NIDS-Net + WA (Ours) + s_{apoc} | 43.9 | 49.6 | 55.6 | 32.8 | 31.5 | 62.0 | 65.0 | 48.6 |

Table 5: Comparison of segmentation performance across various proposal models and embedding generation options. The first row is from CNOS [64].

| Proposal | Embedding | BOP Datasets | | | | | | | Mean |
|----------|----------------|--------------|-------------|-------------|-------------|-------------|-------------|-------------|-------------|
| | | LM-O | T-LESS | TUD-L | IC-BIN | ITODD | HB | YCB-V | |
| SAM | cls token | 39.6 | 39.7 | 39.1 | 28.4 | 28.2 | 48.0 | 59.5 | 40.4 |
| SAM | FFA | 40.0 | 40.0 | 40.8 | 28.0 | 25.8 | 46.0 | 54.4 | 39.3 |
| GS | cls token | 41.7 | 41.7 | 50.8 | 31.5 | 30 | 58 | 63 | 45.2 |
| GS | FFA | 42.9 | 43.0 | 52.0 | 30.5 | 28.8 | 56.6 | 59.7 | 44.8 |
| GS | cls token + WA | 42.5 | 48.2 | 50.7 | 31.3 | 32.0 | 60.5 | 62.8 | 46.9 |
| GS | FFA + WA | 43.2 | 49.2 | 53.5 | 30.5 | 29.4 | 62.4 | 64.3 | 47.5 |

4.4 Ablation Study

Grounded SAM (GS) vs SAM On the seven BOP datasets containing images of numerous cluttered scenes, we compare the object proposals from GS and SAM as detailed in Table 5. The results indicate that GS yields more precise bounding boxes and masks compared to using SAM alone. Furthermore, GS enhances efficiency by eliminating false object proposals, thereby reducing runtime.

FFA vs cls token To compare these two types of embedding generation, we present the results in Table 5. Our weight adapter enhances both two types of embeddings. Despite close segmentation results, FFA produces embeddings that possess greater adaptive potential, demonstrated by higher AP scores after adaption via our weight adapter.

Dinov2 backbones with adapter Our Weight Adapter is compatible with various backbones of Dinov2. Notably, more powerful backbones, which offer a more effective feature space, enable our adapter to deliver greater improvements. Details of this comparison are provided in Table 6. Please refer to the Appendix for additional ablation studies.

Table 6: Detection results using different ViT backbones of Dinov2. “reg” indicates DINOv2 with registers. The results are based on all testing images of the high-resolution dataset. **WA Diff** indicates the improvement attributed to the Weight Adapter.

| Dinov2 backbone | AP | AP50 | AP75 | WA Diff |
|-------------------|------|------|------|----------|
| ViT-S/14 | 47.5 | 56.4 | 51.7 | + 0.9 AP |
| ViT-S/14 + WA | 48.4 | 57.5 | 52.9 | |
| ViT-B/14 | 54.7 | 65.2 | 60.1 | + 3.2 AP |
| ViT-B/14 + WA | 57.9 | 69.0 | 63.6 | |
| ViT-L/14 | 56.8 | 67.7 | 62.3 | + 3.6 AP |
| ViT-L/14 + WA | 60.4 | 71.8 | 66.4 | |
| ViT-L/14 reg | 59.3 | 71.1 | 65.1 | + 4.6 AP |
| ViT-L/14 reg + WA | 63.9 | 76.6 | 70.6 | |

5 Discussions

In this study, we introduce NIDS-Net, a framework designed for novel instance detection and segmentation. We utilize Grounding DINO and SAM to generate precise foreground object proposals, as opposed to conventional naive region proposals. We also present the Weight Adapter, which refines features from a pre-trained vision model effectively and mitigates the risk of overfitting. With the adapter, template and proposal embeddings of different instances are separated to facilitate the subsequent matching. Our method surpasses other approaches significantly in detection performance and also excels in segmentation compared to existing methods.

However, there are limitations: given that our approach incorporates multiple pre-trained models, it requires a longer running time and greater computational resources compared to end-to-end detectors. Additionally, Grounding DINO may produce large bounding boxes that encompass multiple objects, leading to under-segmentation and detection failures. Moreover, our method tends to overlook heavily occluded objects with low confidence scores.

In this work, instances are represented by K template embeddings. For future research, we propose that each instance should be characterized by a single, distinctive embedding that acts as its identifier to enable one-shot detection. This approach will allow the detector to identify and locate a target instance within a query image using just one template image. Additionally, developing an efficient method for this process will be crucial for its application in robotics.

Acknowledgments

This work was supported in part by the DARPA Perceptually-enabled Task Guidance (PTG) Program under contract number HR00112220005.

References

- [1] Sora: Creating video from text. <https://openai.com/sora>. [Accessed Apr 24 2024].
- [2] P. Ammirato, C.-Y. Fu, M. Shvets, J. Kosecka, and A. C. Berg. Target driven instance detection. *arXiv preprint arXiv:1803.04610*, 2018.
- [3] S. F. Bhat, R. Birkel, D. Wofk, P. Wonka, and M. Müller. Zoedepth: Zero-shot transfer by combining relative and metric depth. *arXiv preprint arXiv:2302.12288*, 2023.
- [4] R. Birkel, D. Wofk, and M. Müller. Midas v3. 1—a model zoo for robust monocular relative depth estimation. *arXiv preprint arXiv:2307.14460*, 2023.
- [5] E. Brachmann, A. Krull, F. Michel, S. Gumhold, J. Shotton, and C. Rother. Learning 6d object pose estimation using 3d object coordinates. In *Computer Vision—ECCV 2014: 13th European Conference, Zurich, Switzerland, September 6–12, 2014, Proceedings, Part II 13*, pages 536–551. Springer, 2014.
- [6] T. Brown, B. Mann, N. Ryder, M. Subbiah, J. D. Kaplan, P. Dhariwal, A. Neelakantan, P. Shyam, G. Sastry, A. Askell, et al. Language models are few-shot learners. *Advances in neural information processing systems*, 33:1877–1901, 2020.
- [7] A. Bulat, R. Guerrero, B. Martinez, and G. Tzimiropoulos. Fs-detr: Few-shot detection transformer with prompting and without re-training. In *Proceedings of the IEEE/CVF International Conference on Computer Vision*, pages 11793–11802, 2023.
- [8] B. Calli, A. Singh, A. Walsman, S. Srinivasa, P. Abbeel, and A. M. Dollar. The ycb object and model set: Towards common benchmarks for manipulation research. In *2015 international conference on advanced robotics (ICAR)*, pages 510–517. IEEE, 2015.
- [9] N. Carion, F. Massa, G. Synnaeve, N. Usunier, A. Kirillov, and S. Zagoruyko. End-to-end object detection with transformers. In *European conference on computer vision*, pages 213–229. Springer, 2020.
- [10] M. Caron, H. Touvron, I. Misra, H. Jégou, J. Mairal, P. Bojanowski, and A. Joulin. Emerging properties in self-supervised vision transformers. In *Proceedings of the International Conference on Computer Vision (ICCV)*, 2021.
- [11] M. Caron, H. Touvron, I. Misra, H. Jégou, J. Mairal, P. Bojanowski, and A. Joulin. Emerging properties in self-supervised vision transformers. In *Proceedings of the IEEE/CVF international conference on computer vision*, pages 9650–9660, 2021.
- [12] A. X. Chang, T. Funkhouser, L. Guibas, P. Hanrahan, Q. Huang, Z. Li, S. Savarese, M. Savva, S. Song, H. Su, et al. Shapenet: An information-rich 3d model repository. *arXiv preprint arXiv:1512.03012*, 2015.
- [13] J. Chen, M. Sun, T. Bao, R. Zhao, L. Wu, and Z. He. 3d model-based zero-shot pose estimation pipeline. *arXiv preprint arXiv:2305.17934*, 2023.
- [14] R. Chen, Y. Chen, N. Jiao, and K. Jia. Fantasia3d: Disentangling geometry and appearance for high-quality text-to-3d content creation. In *Proceedings of the IEEE/CVF International Conference on Computer Vision*, pages 22246–22256, 2023.
- [15] T. Chen, S. Kornblith, M. Norouzi, and G. Hinton. A simple framework for contrastive learning of visual representations. In *International conference on machine learning*, pages 1597–1607. PMLR, 2020.

- [16] T. Chen, L. Zhu, C. Deng, R. Cao, Y. Wang, S. Zhang, Z. Li, L. Sun, Y. Zang, and P. Mao. Sam-adapter: Adapting segment anything in underperformed scenes. In *Proceedings of the IEEE/CVF International Conference on Computer Vision*, pages 3367–3375, 2023.
- [17] Z. Chen, Y. Duan, W. Wang, J. He, T. Lu, J. Dai, and Y. Qiao. Vision transformer adapter for dense predictions. *arXiv preprint arXiv:2205.08534*, 2022.
- [18] T. Cheng, L. Song, Y. Ge, W. Liu, X. Wang, and Y. Shan. Yolo-world: Real-time open-vocabulary object detection. *arXiv preprint arXiv:2401.17270*, 2024.
- [19] J. Collins, S. Goel, K. Deng, A. Luthra, L. Xu, E. Gundogdu, X. Zhang, T. F. Y. Vicente, T. Dideriksen, H. Arora, et al. Abo: Dataset and benchmarks for real-world 3d object understanding. In *Proceedings of the IEEE/CVF conference on computer vision and pattern recognition*, pages 21126–21136, 2022.
- [20] T. Darcet, M. Oquab, J. Mairal, and P. Bojanowski. Vision transformers need registers. *arXiv preprint arXiv:2309.16588*, 2023.
- [21] X. Deng, A. Mousavian, Y. Xiang, F. Xia, T. Bretl, and D. Fox. Poserbpf: A rao–blackwellized particle filter for 6-d object pose tracking. *IEEE Transactions on Robotics*, 37(5):1328–1342, 2021.
- [22] M. Denninger, M. Sundermeyer, D. Winkelbauer, Y. Zidan, D. Olefir, M. Elbadrawy, A. Lodhi, and H. Katam. Blenderproc. *arXiv preprint arXiv:1911.01911*, 2019.
- [23] B. Dong, G. Yang, W. Zuo, and L. Zhang. Consept: Continual semantic segmentation via adapter-based vision transformer. *arXiv preprint arXiv:2402.16674*, 2024.
- [24] A. Dosovitskiy, L. Beyer, A. Kolesnikov, D. Weissenborn, X. Zhai, T. Unterthiner, M. Dehghani, M. Minderer, G. Heigold, S. Gelly, et al. An image is worth 16x16 words: Transformers for image recognition at scale. *arXiv preprint arXiv:2010.11929*, 2020.
- [25] A. Doumanoglou, R. Kouskouridas, S. Malassiotis, and T.-K. Kim. Recovering 6d object pose and predicting next-best-view in the crowd. In *Proceedings of the IEEE conference on computer vision and pattern recognition*, pages 3583–3592, 2016.
- [26] B. Drost, M. Ulrich, P. Bergmann, P. Hartinger, and C. Steger. Introducing mvtec itodd-a dataset for 3d object recognition in industry. In *Proceedings of the IEEE international conference on computer vision workshops*, pages 2200–2208, 2017.
- [27] J. Du, S. Zhang, Q. Chen, H. Le, Y. Sun, Y. Ni, J. Wang, B. He, and J. Wang. σ -adaptive decoupled prototype for few-shot object detection. In *2023 IEEE/CVF International Conference on Computer Vision (ICCV)*, pages 18904–18914. IEEE, 2023.
- [28] P. Gao, S. Geng, R. Zhang, T. Ma, R. Fang, Y. Zhang, H. Li, and Y. Qiao. Clip-adapter: Better vision-language models with feature adapters. *arXiv 2110.04544*, 2021.
- [29] P. Gao, J. Han, R. Zhang, Z. Lin, S. Geng, A. Zhou, W. Zhang, P. Lu, C. He, X. Yue, H. Li, and Y. Qiao. Llama-adapter v2: Parameter-efficient visual instruction model. *arXiv preprint arXiv:2304.15010*, 2023.
- [30] R. Girshick. Fast r-cnn. In *Proceedings of the IEEE international conference on computer vision*, pages 1440–1448, 2015.
- [31] X. Han, L. Wei, X. Yu, Z. Dou, X. He, K. Wang, Z. Han, and Q. Tian. Boosting segment anything model towards open-vocabulary learning. *arXiv preprint arXiv:2312.03628*, 2023.
- [32] K. He, X. Zhang, S. Ren, and J. Sun. Deep residual learning for image recognition. In *Proceedings of the IEEE conference on computer vision and pattern recognition*, pages 770–778, 2016.
- [33] K. He, G. Gkioxari, P. Dollár, and R. Girshick. Mask r-cnn. In *Proceedings of the IEEE international conference on computer vision*, pages 2961–2969, 2017.

- [34] T. Hodan, P. Haluza, Š. Obdržálek, J. Matas, M. Lourakis, and X. Zabulis. T-less: An rgb-d dataset for 6d pose estimation of texture-less objects. In *2017 IEEE Winter Conference on Applications of Computer Vision (WACV)*, pages 880–888. IEEE, 2017.
- [35] T. Hodan, F. Michel, E. Brachmann, W. Kehl, A. GlentBuch, D. Kraft, B. Drost, J. Vidal, S. Ihrke, X. Zabulis, et al. Bop: Benchmark for 6d object pose estimation. In *Proceedings of the European conference on computer vision (ECCV)*, pages 19–34, 2018.
- [36] E. J. Hu, Y. Shen, P. Wallis, Z. Allen-Zhu, Y. Li, S. Wang, L. Wang, and W. Chen. Lora: Low-rank adaptation of large language models. *arXiv preprint arXiv:2106.09685*, 2021.
- [37] Z. Hu, L. Wang, Y. Lan, W. Xu, E.-P. Lim, L. Bing, X. Xu, S. Poria, and R. K.-W. Lee. Llm-adapters: An adapter family for parameter-efficient fine-tuning of large language models. *arXiv preprint arXiv:2304.01933*, 2023.
- [38] R. Kaskman, S. Zakharov, I. Shugurov, and S. Ilic. Homebreweddb: Rgb-d dataset for 6d pose estimation of 3d objects. In *Proceedings of the IEEE/CVF International Conference on Computer Vision Workshops*, pages 0–0, 2019.
- [39] D. Kim, T.-Y. Lin, A. Angelova, I. S. Kweon, and W. Kuo. Learning open-world object proposals without learning to classify. *IEEE Robotics and Automation Letters*, 7(2):5453–5460, 2022.
- [40] D. Kim, A. Angelova, and W. Kuo. Detection-oriented image-text pretraining for open-vocabulary detection. *arXiv preprint arXiv:2310.00161*, 2023.
- [41] D. Kim, A. Angelova, and W. Kuo. Region-aware pretraining for open-vocabulary object detection with vision transformers. In *Proceedings of the IEEE/CVF Conference on Computer Vision and Pattern Recognition*, pages 11144–11154, 2023.
- [42] A. Kirillov, E. Mintun, N. Ravi, H. Mao, C. Rolland, L. Gustafson, T. Xiao, S. Whitehead, A. C. Berg, W.-Y. Lo, et al. Segment anything. In *Proceedings of the IEEE/CVF International Conference on Computer Vision*, pages 4015–4026, 2023.
- [43] A. Kirillov, E. Mintun, N. Ravi, H. Mao, C. Rolland, L. Gustafson, T. Xiao, S. Whitehead, A. C. Berg, W.-Y. Lo, et al. Segment anything. In *Proceedings of the IEEE/CVF International Conference on Computer Vision*, pages 4015–4026, 2023.
- [44] K. Kotar, S. Tian, H.-X. Yu, D. Yamins, and J. Wu. Are these the same apple? comparing images based on object intrinsics. *Advances in Neural Information Processing Systems*, 36, 2024.
- [45] B. Li, J. Wang, Y. Hu, C. Wang, and S. Scherer. Voxdet: Voxel learning for novel instance detection. *Advances in Neural Information Processing Systems*, 36, 2024.
- [46] X. Li, X. Yin, C. Li, P. Zhang, X. Hu, L. Zhang, L. Wang, H. Hu, L. Dong, F. Wei, et al. Oscar: Object-semantics aligned pre-training for vision-language tasks. In *Computer Vision–ECCV 2020: 16th European Conference, Glasgow, UK, August 23–28, 2020, Proceedings, Part XXX 16*, pages 121–137. Springer, 2020.
- [47] Y. Li, G. Wang, X. Ji, Y. Xiang, and D. Fox. Deepim: Deep iterative matching for 6d pose estimation. In *Proceedings of the European Conference on Computer Vision (ECCV)*, pages 683–698, 2018.
- [48] C.-H. Lin, J. Gao, L. Tang, T. Takikawa, X. Zeng, X. Huang, K. Kreis, S. Fidler, M.-Y. Liu, and T.-Y. Lin. Magic3d: High-resolution text-to-3d content creation. In *Proceedings of the IEEE/CVF Conference on Computer Vision and Pattern Recognition*, pages 300–309, 2023.
- [49] J. Lin, L. Liu, D. Lu, and K. Jia. Sam-6d: Segment anything model meets zero-shot 6d object pose estimation. *arXiv preprint arXiv:2311.15707*, 2023.
- [50] T.-Y. Lin, M. Maire, S. Belongie, J. Hays, P. Perona, D. Ramanan, P. Dollár, and C. L. Zitnick. Microsoft coco: Common objects in context. In *Computer Vision–ECCV 2014: 13th European Conference, Zurich, Switzerland, September 6–12, 2014, Proceedings, Part V 13*, pages 740–755. Springer, 2014.

- [51] T.-Y. Lin, P. Goyal, R. Girshick, K. He, and P. Dollár. Focal loss for dense object detection. In *Proceedings of the IEEE international conference on computer vision*, pages 2980–2988, 2017.
- [52] S. Liu, Z. Zeng, T. Ren, F. Li, H. Zhang, J. Yang, C. Li, J. Yang, H. Su, J. Zhu, et al. Grounding dino: Marrying dino with grounded pre-training for open-set object detection. *arXiv preprint arXiv:2303.05499*, 2023.
- [53] Y. Liu, Y. Wen, S. Peng, C. Lin, X. Long, T. Komura, and W. Wang. Gen6d: Generalizable model-free 6-dof object pose estimation from rgb images. In *European Conference on Computer Vision*, pages 298–315. Springer, 2022.
- [54] Z. Liu, Y. Lin, Y. Cao, H. Hu, Y. Wei, Z. Zhang, S. Lin, and B. Guo. Swin transformer: Hierarchical vision transformer using shifted windows. In *Proceedings of the IEEE/CVF international conference on computer vision*, pages 10012–10022, 2021.
- [55] Z. Liu, H. Mao, C.-Y. Wu, C. Feichtenhofer, T. Darrell, and S. Xie. A convnet for the 2020s. In *Proceedings of the IEEE/CVF conference on computer vision and pattern recognition*, pages 11976–11986, 2022.
- [56] X. Lu, W. Diao, Y. Mao, J. Li, P. Wang, X. Sun, and K. Fu. Breaking immutable: Information-coupled prototype elaboration for few-shot object detection. In *Proceedings of the AAAI Conference on Artificial Intelligence*, volume 37, pages 1844–1852, 2023.
- [57] Y. Lu, Y. Chen, N. Ruozzi, and Y. Xiang. Mean shift mask transformer for unseen object instance segmentation. *arXiv preprint arXiv:2211.11679*, 2022.
- [58] Y. Lu, N. Khargonkar, Z. Xu, C. Averill, K. Palanisamy, K. Hang, Y. Guo, N. Ruozzi, and Y. Xiang. Self-supervised unseen object instance segmentation via long-term robot interaction. *arXiv preprint arXiv:2302.03793*, 2023.
- [59] J. Ma, Y. Niu, J. Xu, S. Huang, G. Han, and S.-F. Chang. Digeo: Discriminative geometry-aware learning for generalized few-shot object detection. In *Proceedings of the IEEE/CVF Conference on Computer Vision and Pattern Recognition*, pages 3208–3218, 2023.
- [60] D. G. McVitie and L. B. Wilson. The stable marriage problem. *Communications of the ACM*, 14(7):486–490, 1971.
- [61] J.-P. Mercier, M. Garon, P. Giguere, and J.-F. Lalonde. Deep template-based object instance detection. In *Proceedings of the IEEE/CVF Winter Conference on Applications of Computer Vision*, pages 1507–1516, 2021.
- [62] J.-P. Mercier, M. Garon, P. Giguere, and J.-F. Lalonde. Deep template-based object instance detection. In *Proceedings of the IEEE/CVF Winter Conference on Applications of Computer Vision*, pages 1507–1516, 2021.
- [63] M. Minderer, A. Gritsenko, A. Stone, M. Neumann, D. Weissenborn, A. Dosovitskiy, A. Mahendran, A. Arnab, M. Dehghani, Z. Shen, et al. Simple open-vocabulary object detection with vision transformers. *arxiv 2022. arXiv preprint arXiv:2205.06230*, 2, 2022.
- [64] V. N. Nguyen, T. Groueix, G. Ponimatin, V. Lepetit, and T. Hodan. Cnos: A strong baseline for cad-based novel object segmentation. In *Proceedings of the IEEE/CVF International Conference on Computer Vision*, pages 2134–2140, 2023.
- [65] A. v. d. Oord, Y. Li, and O. Vinyals. Representation learning with contrastive predictive coding. *arXiv preprint arXiv:1807.03748*, 2018.
- [66] M. Oquab, T. Darcet, T. Moutakanni, H. Vo, M. Szafraniec, V. Khalidov, P. Fernandez, D. Haziza, F. Massa, A. El-Nouby, et al. Dinov2: Learning robust visual features without supervision. *arXiv preprint arXiv:2304.07193*, 2023.
- [67] A. Osokin, D. Sumin, and V. Lomakin. Os2d: One-stage one-shot object detection by matching anchor features. In *Computer Vision—ECCV 2020: 16th European Conference, Glasgow, UK, August 23–28, 2020, Proceedings, Part XV 16*, pages 635–652. Springer, 2020.

- [68] J. J. P. K. Palanisamy, Y.-W. Chao, X. Du, and Y. Xiang. Proto-clip: Vision-language prototypical network for few-shot learning. 2023.
- [69] X. Pu, H. Jia, L. Zheng, F. Wang, and F. Xu. Classwise-sam-adapter: Parameter efficient fine-tuning adapts segment anything to sar domain for semantic segmentation. *arXiv preprint arXiv:2401.02326*, 2024.
- [70] A. Radford, K. Narasimhan, T. Salimans, and I. Sutskever. Improving language understanding with unsupervised learning. 2018.
- [71] A. Radford, J. Wu, R. Child, D. Luan, D. Amodei, I. Sutskever, et al. Language models are unsupervised multitask learners. *OpenAI blog*, 1(8):9, 2019.
- [72] A. Radford, J. W. Kim, C. Hallacy, A. Ramesh, G. Goh, S. Agarwal, G. Sastry, A. Askell, P. Mishkin, J. Clark, et al. Learning transferable visual models from natural language supervision. In *International conference on machine learning*, pages 8748–8763. PMLR, 2021.
- [73] A. Radford, J. W. Kim, C. Hallacy, A. Ramesh, G. Goh, S. Agarwal, G. Sastry, A. Askell, P. Mishkin, J. Clark, et al. Learning transferable visual models from natural language supervision. In *International conference on machine learning*, pages 8748–8763. PMLR, 2021.
- [74] A. Raj, S. Kaza, B. Poole, M. Niemeyer, N. Ruiz, B. Mildenhall, S. Zada, K. Aberman, M. Rubinstein, J. Barron, et al. Dreambooth3d: Subject-driven text-to-3d generation. In *Proceedings of the IEEE/CVF International Conference on Computer Vision*, pages 2349–2359, 2023.
- [75] J. Redmon, S. Divvala, R. Girshick, and A. Farhadi. You only look once: Unified, real-time object detection. In *Proceedings of the IEEE conference on computer vision and pattern recognition*, pages 779–788, 2016.
- [76] S. Ren, K. He, R. Girshick, and J. Sun. Faster r-cnn: Towards real-time object detection with region proposal networks. *Advances in neural information processing systems*, 28, 2015.
- [77] S. Ren, K. He, R. Girshick, and J. Sun. Faster r-cnn: Towards real-time object detection with region proposal networks. *Advances in neural information processing systems*, 28, 2015.
- [78] T. Ren, S. Liu, A. Zeng, J. Lin, K. Li, H. Cao, J. Chen, X. Huang, Y. Chen, F. Yan, et al. Grounded sam: Assembling open-world models for diverse visual tasks. *arXiv preprint arXiv:2401.14159*, 2024.
- [79] Q. Shen, Y. Zhao, N. Kwon, J. Kim, Y. Li, and S. Kong. A high-resolution dataset for instance detection with multi-view instance capture. In *NeurIPS Datasets and Benchmarks Track*, 2023.
- [80] U. Singer, A. Polyak, T. Hayes, X. Yin, J. An, S. Zhang, Q. Hu, H. Yang, O. Ashual, O. Gafni, et al. Make-a-video: Text-to-video generation without text-video data. *arXiv preprint arXiv:2209.14792*, 2022.
- [81] L. Song, R. Xue, H. Wang, H. Sun, Y. Ge, Y. Shan, et al. Meta-adapter: An online few-shot learner for vision-language model. *Advances in Neural Information Processing Systems*, 36, 2024.
- [82] M. Sundermeyer, T. Hodaň, Y. Labbe, G. Wang, E. Brachmann, B. Drost, C. Rother, and J. Matas. Bop challenge 2022 on detection, segmentation and pose estimation of specific rigid objects. In *Proceedings of the IEEE/CVF Conference on Computer Vision and Pattern Recognition*, pages 2784–2793, 2023.
- [83] Z. Tian, C. Shen, H. Chen, and T. He. Fcos: Fully convolutional one-stage object detection. In *2019 IEEE/CVF International Conference on Computer Vision (ICCV)*, pages 9626–9635, 2019. doi: 10.1109/ICCV.2019.00972.
- [84] H. Touvron, T. Lavril, G. Izacard, X. Martinet, M.-A. Lachaux, T. Lacroix, B. Rozière, N. Goyal, E. Hambro, F. Azhar, et al. Llama: Open and efficient foundation language models. *arXiv preprint arXiv:2302.13971*, 2023.

- [85] B. Wen, W. Yang, J. Kautz, and S. Birchfield. Foundationpose: Unified 6d pose estimation and tracking of novel objects. *arXiv preprint arXiv:2312.08344*, 2023.
- [86] Y. Wu, A. Kirillov, F. Massa, W.-Y. Lo, and R. Girshick. Detectron2. <https://github.com/facebookresearch/detectron2>, 2019.
- [87] Y. Xiang, T. Schmidt, V. Narayanan, and D. Fox. Posecnn: A convolutional neural network for 6d object pose estimation in cluttered scenes. *arXiv preprint arXiv:1711.00199*, 2017.
- [88] Y. Xiang, C. Xie, A. Mousavian, and D. Fox. Learning rgb-d feature embeddings for unseen object instance segmentation. In *Conference on Robot Learning*, pages 461–470. PMLR, 2021.
- [89] C. Xie, Y. Xiang, A. Mousavian, and D. Fox. Unseen object instance segmentation for robotic environments. *IEEE Transactions on Robotics*, 37(5):1343–1359, 2021.
- [90] S. Xie, R. Girshick, P. Dollár, Z. Tu, and K. He. Aggregated residual transformations for deep neural networks. In *Proceedings of the IEEE conference on computer vision and pattern recognition*, pages 1492–1500, 2017.
- [91] Z. Xie, B. Guan, W. Jiang, M. Yi, Y. Ding, H. Lu, and L. Zhang. Pa-sam: Prompt adapter sam for high-quality image segmentation. *2024 IEEE International Conference on Multimedia and Expo (ICME)*, 2024.
- [92] J. Xu, H. Le, and D. Samaras. Generating features with increased crop-related diversity for few-shot object detection. In *Proceedings of the IEEE/CVF Conference on Computer Vision and Pattern Recognition*, pages 19713–19722, 2023.
- [93] J. Xu, X. Wang, W. Cheng, Y.-P. Cao, Y. Shan, X. Qie, and S. Gao. Dream3d: Zero-shot text-to-3d synthesis using 3d shape prior and text-to-image diffusion models. In *Proceedings of the IEEE/CVF Conference on Computer Vision and Pattern Recognition*, pages 20908–20918, 2023.
- [94] H. Yang, S. Cai, H. Sheng, B. Deng, J. Huang, X.-S. Hua, Y. Tang, and Y. Zhang. Balanced and hierarchical relation learning for one-shot object detection. In *Proceedings of the IEEE/CVF conference on computer vision and pattern recognition*, pages 7591–7600, 2022.
- [95] L. Yang, B. Kang, Z. Huang, X. Xu, J. Feng, and H. Zhao. Depth anything: Unleashing the power of large-scale unlabeled data. *arXiv preprint arXiv:2401.10891*, 2024.
- [96] H. Zhang, F. Li, S. Liu, L. Zhang, H. Su, J. Zhu, L. M. Ni, and H.-Y. Shum. Dino: Detr with improved denoising anchor boxes for end-to-end object detection, 2022.
- [97] R. Zhang, Z. Wei, R. Fang, P. Gao, K. Li, J. Dai, Y. Qiao, and H. Li. Tip-adapter: Training-free adaption of clip for few-shot classification. *arXiv preprint arXiv:2207.09519*, 2022.
- [98] R. Zhang, J. Han, C. Liu, P. Gao, A. Zhou, X. Hu, S. Yan, P. Lu, H. Li, and Y. Qiao. Llama-adapter: Efficient fine-tuning of language models with zero-init attention. *arXiv preprint arXiv:2303.16199*, 2023.
- [99] R. Zhang, X. Hu, B. Li, S. Huang, H. Deng, Y. Qiao, P. Gao, and H. Li. Prompt, generate, then cache: Cascade of foundation models makes strong few-shot learners. In *Proceedings of the IEEE/CVF Conference on Computer Vision and Pattern Recognition*, pages 15211–15222, 2023.
- [100] X. Zhang, Y. Wang, and A. Boularias. Detect everything with few examples, 2024.
- [101] X. Zhao, W. Ding, Y. An, Y. Du, T. Yu, M. Li, M. Tang, and J. Wang. Fast segment anything. *arXiv preprint arXiv:2306.12156*, 2023.
- [102] X. Zhou, D. Wang, and P. Krähenbühl. Objects as points. *arXiv preprint arXiv:1904.07850*, 2019.

6 Appendix / supplemental material

6.1 Training Details

Detection. For detection datasets, the weight adapter is trained with a batch size of 1024, while the CLIP-Adapter is trained with a batch size of 512 to enhance performance. Both adapters are trained for the same number of epochs, as detailed in Table 7. To utilize Grounding DINO, a box threshold of 0.15 is set for the high-resolution and YCB-V datasets, and 0.10 for other datasets.

Table 7: The training epochs of different detection datasets.

| | High-resolution | RoboTools | LM-O | YCB-V |
|---------------|-----------------|-----------|------|-------|
| Both Adapters | 40 | 80 | 40 | 40 |

Segmentation. We combine all instances from seven core datasets of the BOP benchmark. We train both adapters with a batch size of 1344 (32 instances \times 42 templates per instance) for 500 epochs. For Grounding DINO, a box threshold of 0.10 is set for all datasets.

6.2 More Ablation Study

FFA vs *cls* token and Grounded SAM (GS) vs SAM in Detection Tasks. The detection capabilities of FFA and the *cls* token are demonstrated using the high-resolution dataset, as presented in Table 8. For instance embedding generation, FFA achieves significantly greater enhancements compared to the *cls* token. Furthermore, Table 8 illustrates that GS is effective in generating precise object proposals.

Table 8: The detection results on all images of the high-resolution dataset. “Proposal” refers to the object proposal method. “Embedding” denotes the method of instance embedding generation.

| Proposal | Embedding | AP | AP50 | AP75 |
|----------|------------------|-------------|-------------|-------------|
| SAM | <i>cls</i> token | 41.6 | 49.1 | 46.0 |
| GS | <i>cls</i> token | 54.9 | 65.4 | 60.1 |
| GS | FFA | 59.3 | 71.1 | 65.1 |

Aggregation. For *cls* token embeddings, averaging the top k highest (*avg k*) scores yields the best results [64, 49]. For FFA embeddings, the max aggregation function achieves optimal outcomes. The comparison of these aggregation functions is detailed in Table 9.

Table 9: Comparison of aggregation functions for segmentation performance. We report Average Precision (AP). *avg k* refers to averaging the top k scores. All results are based on object proposals from Grounded SAM (GS).

| Embedding | Aggregation | BOP Datasets | | | | | | | Mean |
|------------------|--------------|--------------|-------------|-------------|-------------|-------------|-------------|-------------|-------------|
| | | LM-O | T-LESS | TUD-L | IC-BIN | ITODD | HB | YCB-V | |
| <i>cls</i> token | <i>avg k</i> | 41.7 | 41.7 | 50.8 | 31.5 | 30 | 58 | 63 | 45.2 |
| <i>cls</i> token | max | 42 | 37.4 | 45.9 | 30.2 | 28.9 | 54.9 | 61.5 | 43.0 |
| FFA | <i>avg k</i> | 42.5 | 42 | 47.4 | 28.2 | 27.3 | 55.1 | 61.5 | 43.4 |
| FFA | max | 42.9 | 43 | 52 | 30.5 | 28.8 | 56.6 | 59.7 | 44.8 |

Runtime. We compare the efficiency of existing methods for novel instance segmentation, as presented in Table 10. Our approach significantly reduces running time by proposing only high-quality bounding boxes.

6.3 Unseen Detection of BOP Benchmark

We compare our approach with ZeroPose [13], CNOS [64], and SAM-6D [49] for 2D unseen detection, as illustrated in Table 11. Our method outperforms the best RGB method by 2.5 AP and competes effectively with the top RGB-D method.

Table 10: Runtime comparisons of various methods for novel instance segmentation.

| Method | Proposal | Server | Time (sec) |
|-----------------------------------|----------|------------------|------------|
| CNOS | FastSAM | Tesla V100 | 0.22 |
| CNOS | | DeForce RTX 3090 | 0.23 |
| SAM-6D (RGB) | | DeForce RTX 3090 | 0.25 |
| SAM-6D (RGBD) | | DeForce RTX 3090 | 0.45 |
| CNOS | SAM | Tesla V100 | 1.84 |
| CNOS | | DeForce RTX 3090 | 2.35 |
| SAM-6D (RGB) | | DeForce RTX 3090 | 2.28 |
| SAM-6D (RGBD) | | DeForce RTX 3090 | 2.80 |
| NIDS-Net (Ours) | GS | RTX A5000 | 0.49 |
| NIDS-Net + CA (Ours) | | | 0.48 |
| NIDS-Net + WA (Ours) | | | 0.48 |
| NIDS-Net + WA + s_{appe} (Ours) | | | 0.48 |

Table 11: Unseen instance detection results across the seven core datasets of the BOP benchmark, with all results reported as Average Precision (AP).

| Method | Proposal | BOP Datasets | | | | | | | |
|-----------------------------------|----------|--------------|-------------|-------------|-------------|-------------|-------------|-------------|-------------|
| | | LM-O | T-LESS | TUD-L | IC-BIN | ITODD | HB | YCB-V | Mean |
| ZeroPose [13] | SAM | 36.7 | 30.0 | 43.1 | 22.8 | 25.0 | 39.8 | 41.6 | 34.1 |
| CNOS | SAM | 39.5 | 33.0 | 36.8 | 20.7 | 31.3 | 42.3 | 49.0 | 36.1 |
| CNOS [64] | FastSAM | 43.3 | 39.5 | 53.4 | 22.6 | 32.5 | 51.7 | 56.8 | 42.8 |
| SAM-6D (RGB) [49] | FastSAM | 43.8 | 41.7 | 54.6 | 23.4 | 37.4 | 52.3 | 57.3 | 44.4 |
| SAM-6D (RGBD) [49] | SAM | 46.6 | 43.7 | 53.7 | 26.1 | 39.3 | 53.1 | 51.9 | 44.9 |
| SAM-6D (RGBD) [49] | FastSAM | 46.3 | 45.8 | 57.3 | 24.5 | 41.9 | 55.1 | 58.9 | 47.1 |
| NIDS-Net (Ours) | GS | 44.9 | 42.8 | 43.4 | 24.4 | 34.9 | 54.8 | 56.5 | 43.1 |
| NIDS-Net + WA(Ours) | | 44.9 | 48.9 | 46.0 | 24.5 | 36.0 | 59.4 | 62.4 | 46.0 |
| NIDS-Net + WA (Ours) + s_{appe} | | 45.7 | 49.3 | 48.6 | 25.7 | 37.9 | 58.7 | 62.1 | 46.9 |

6.4 More Qualitative Results

6.4.1 Adapter

To facilitate a comparison between the CLIP-Adapter and our Weight Adapter, we present a visual illustration in Figure 4. It is evident that the CLIP-Adapter alters the feature space and spoils the embeddings of background objects due to overfitting. In contrast, our Weight Adapter delivers robust embeddings within the original feature space.

6.4.2 Detection

We display the visual outcomes of our methodology employing the weight adapter on the LMO and YCB-V datasets in Figure 5. The gap between synthetic and real images results in some instances of detection failure. For example, some LM-O instances are not found with our method.

6.4.3 Segmentation

We present the visual outcomes of our approach using the weight adapter on the BoP datasets in Figures 6, 7, 8, and 9. These images demonstrate the effectiveness of our approach in cluttered environments. In some cases of T-LESS and IC-BIN datasets, Grounding DINO generates large bounding boxes which include multiple objects, causing under-segmentation. Furthermore, in IC-BIN and HB datasets, some heavily occluded objects with low confidence scores are overlooked by our method.

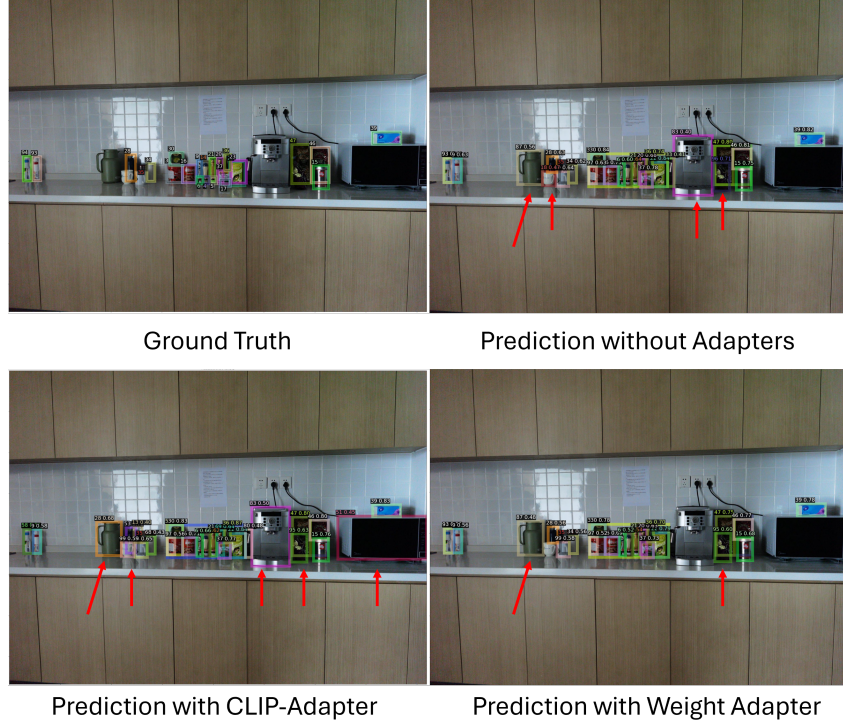


Figure 4: Comparison of different adapters on a hard scene image from the high-resolution dataset. Red arrows denote background objects that are erroneously classified as targets.

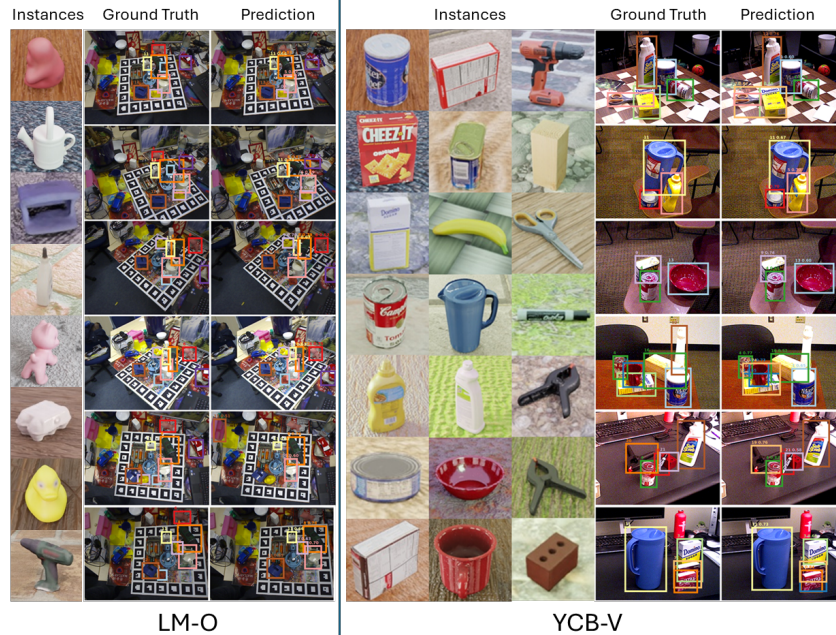


Figure 5: Visual detection results using the Weight Adapter on the LM-O and YCB-V datasets. Our approach detects object instances according to their synthetic template images.

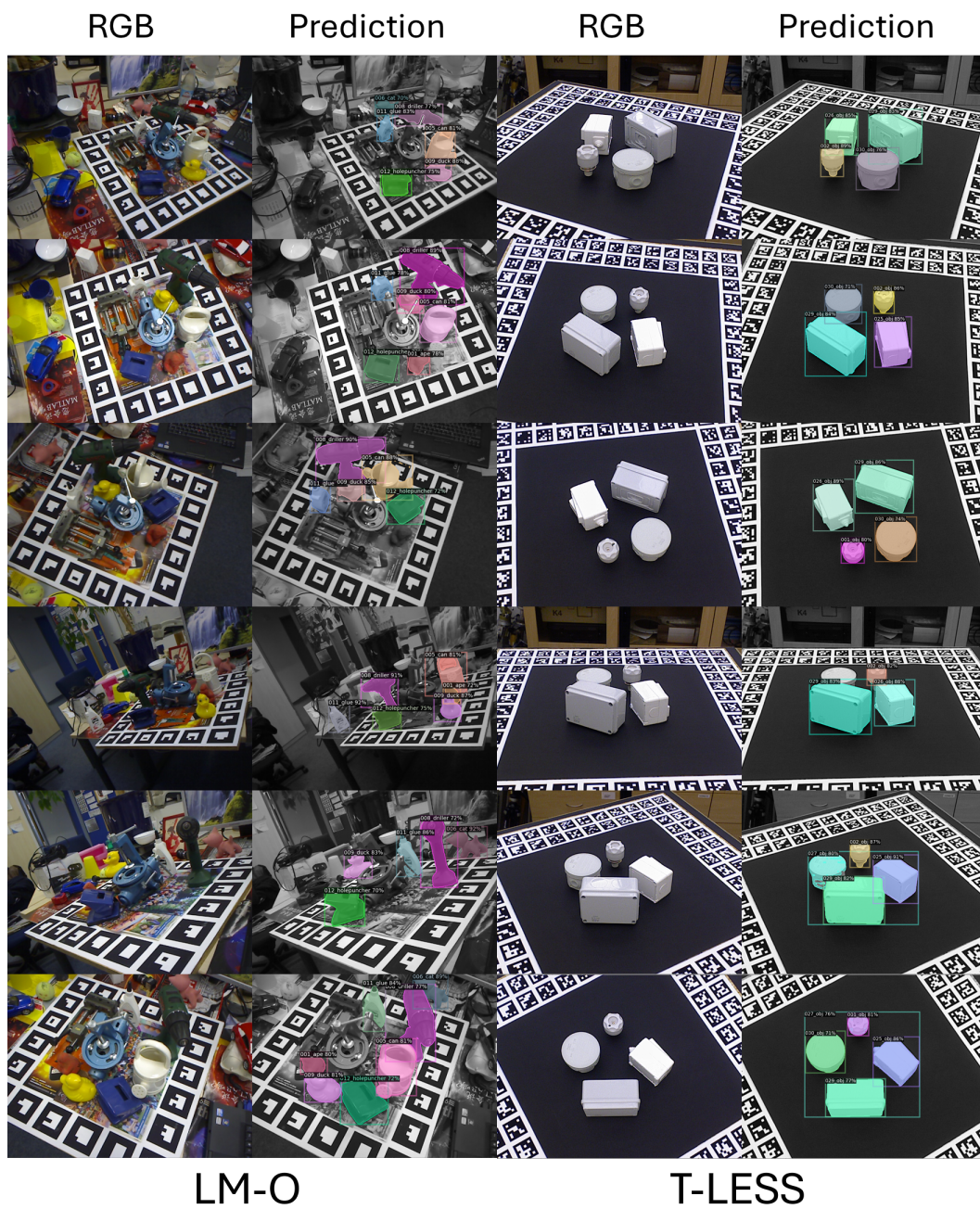


Figure 6: Qualitative segmentation results on the LM-O and T-Less datasets.

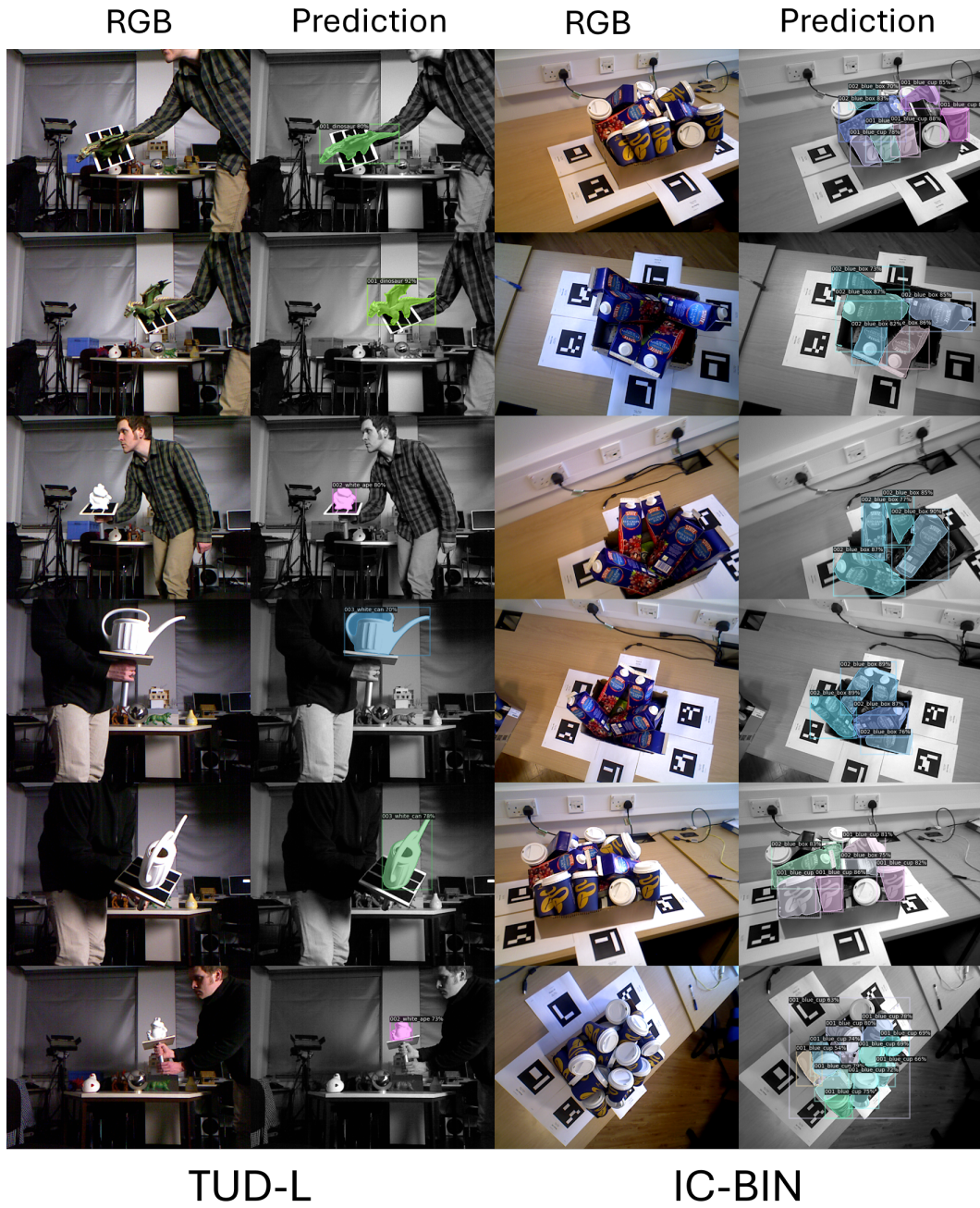


Figure 7: Qualitative segmentation results on the TUD-L and IC-BIN datasets.

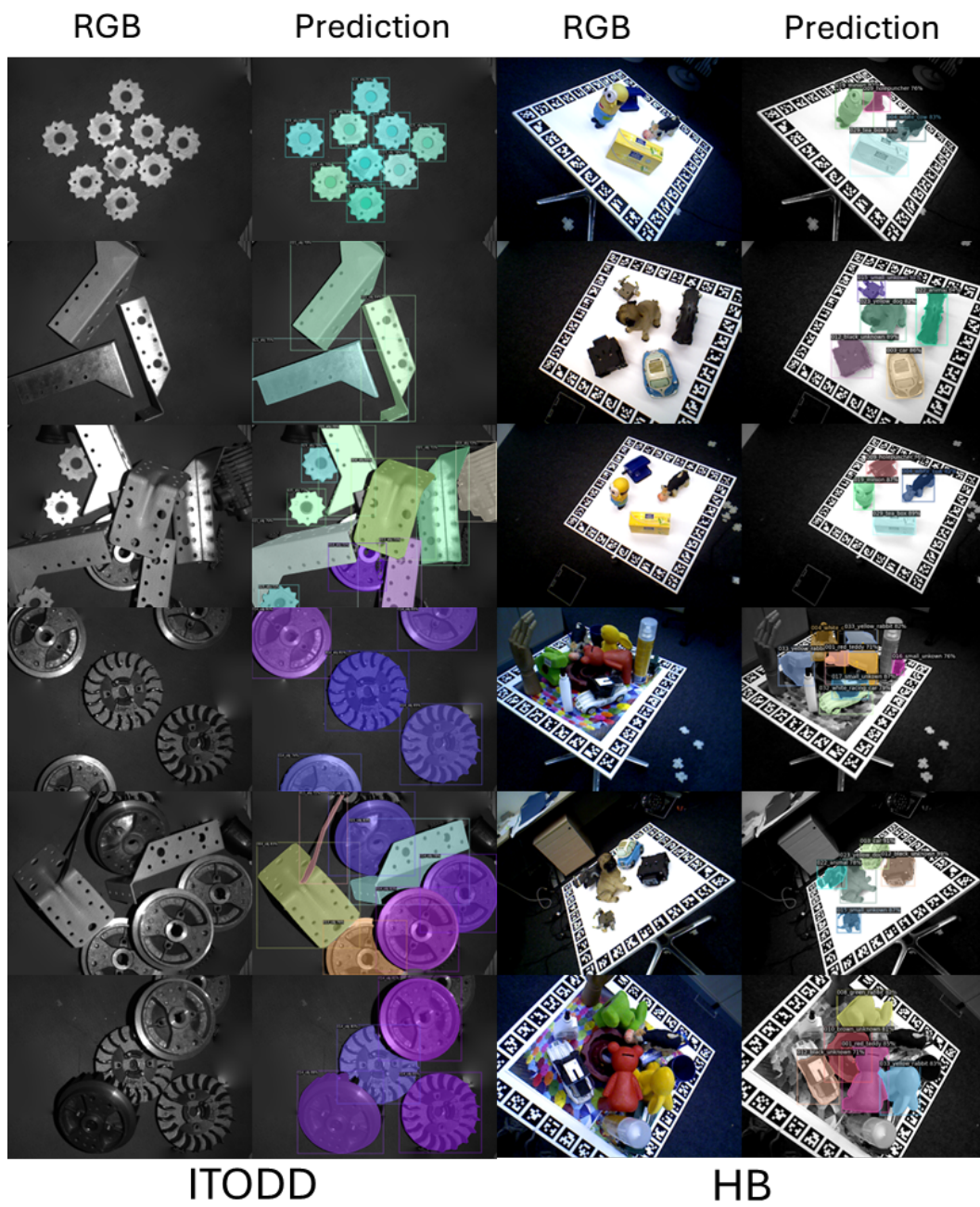


Figure 8: Qualitative segmentation results on the ITODD and HB datasets

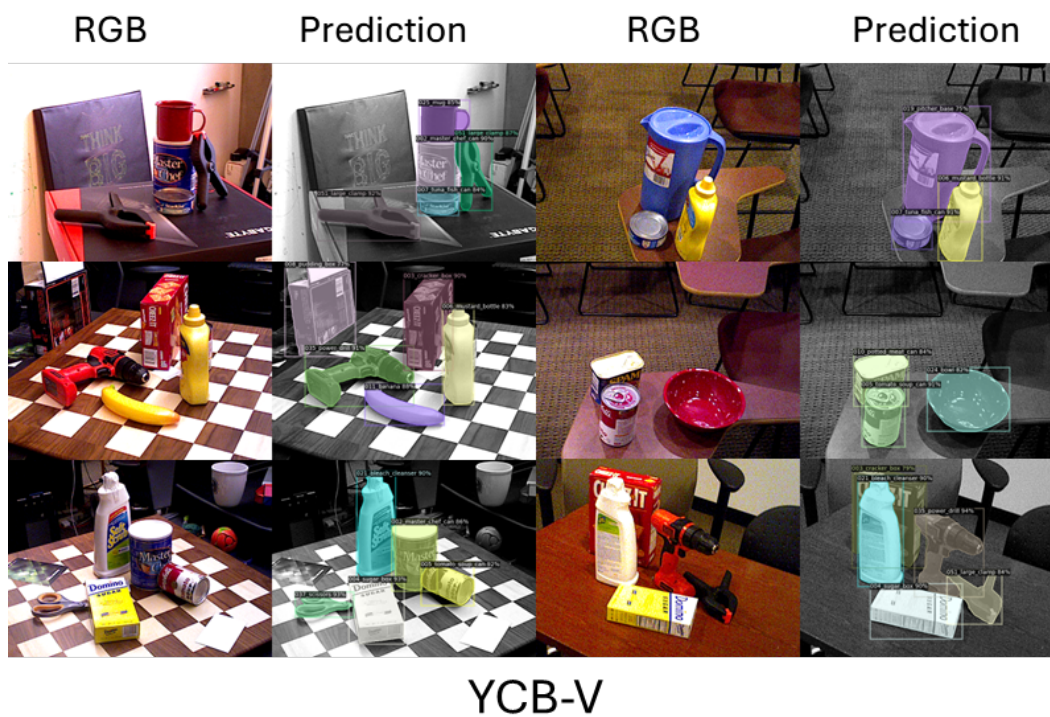


Figure 9: Qualitative segmentation results on the YCB-V dataset.